



RESEARCH ARTICLE

Design of a flexible robot toward transbronchial lung biopsy

Runtian Zhang^{1,2} , Dongsheng Xie^{2,3} , Chao Qian^{1,2}, Xingguang Duan^{1,2,3} and Changsheng Li^{1,2,*}

¹School of Mechatronic Engineering, Beijing Institute of Technology, Beijing 100081, China, ²Advanced Innovation Center for Intelligent Robots and Systems, Beijing Institute of Technology, Beijing 100081, China, and ³Institute of Engineering Medicine, Beijing Institute of Technology, Beijing 100081, China

*Corresponding author. E-mail: lics@bit.edu.cn

Received: 29 March 2022; **Revised:** 15 July 2022; **Accepted:** 23 August 2022; **First published online:** 27 September 2022

Keywords: surgical robotics, transbronchial lung biopsy, cable-driven mechanism, flexible mechanism

Abstract

Transbronchial lung biopsy is an effective and less-invasive treatment for the early diagnosis of lung cancer. However, the limited dexterity of existing endoscopic instruments and the complexity of bronchial access prevent the application of such procedures mainly for biopsy and diagnosis. This paper proposes a flexible robot for transbronchial lung biopsy with a cable-driven mechanism-based flexible manipulator. The robotic system of transbronchial lung biopsy is presented in detail, including the snake-bone end effector, the flexible catheters and the actuation unit. The kinematic analysis of the snake-bone end effector is conducted for the master-slave control. The experimental results show that the end effector reaches the target nodule through a narrow and tortuous pathway in a bronchial model. In conclusion, the proposed robotic system contributes to the field of advanced endoscopic surgery with high flexibility and controllability.

1. Introduction

Only 15% of all diagnosed lung cancers are detected at an early stage at present, which causes a five-year survival rate of only 16% [1]. The delay in diagnosis and treatment is, therefore, the main reason for the high mortality of lung cancer [2]. Clinically, the diagnosis of lung cancer is based on the existence of pulmonary nodules (a kind of nearly spherical tissue with high density) and their biological features observed from CT images [3]. With screening and early intervention, the survival rate of lung cancer can be significantly improved [4]. More specifically, the detection and treatment of lung nodules in early stages of growth can contribute to saving more lives [5].

The challenge is to distinguish between benign and malignant nodules with a noninvasive method [3]. There is actually a small range of choices concerning the diagnostic methods on the pulmonary nodules [6]. The characteristic information provided by conventional imaging techniques can only provide limited characteristic information, which makes it difficult to evaluate the malignancy of nodules by visual inspection. Therefore, its clinical value lies mainly in the preliminary diagnosis [7]. Although several progress has been made in recent years on the reduction of false negative rate of pulmonary nodules by improving the algorithm of medical image processing [8, 9, 10, 11], the result is still unsatisfying. In clinical practice, sampling biopsy, which serves as a complement to the imaging-based diagnosis, is usually conducted after the conventional X-ray chest film checking to improve diagnostic accuracy and reliability cite2013Multimodal.

Sampling biopsy is the key to judge pathology accurately. Currently, the least invasive and most common procedures for biopsy are percutaneous and transoral bronchoscopic biopsy [12], both of

which possess limitations. Percutaneous puncture biopsy can reach the surrounding lungs with pleural puncture, which may lead to the incidence of pneumothorax (lung collapse) as high as 25% [13]. Transoral bronchoscopic biopsy can reduce the surgical trauma and avoid the related complications of patients. However, due to the narrow internal space of human bronchus and the complex distribution network of bronchi, it is difficult to reach the deep lesions of bronchus by conventional manual operation of bronchoscope [14, 15, 16]. Hence, the conventional biopsy is developed toward the robot-assisted one with high precision and instantaneity [17, 18].

Medical robotics are capable of conducting minimally invasive interventions on internal organs located in confined areas [15, 19, 20, 21, 22, 23, 24, 25]. Relevant scholars have also worked on robot-assisted transbronchial lung biopsy [14, 26, 27]. In this paper, taking a different approach, a flexible robot with minimized end effector diameter, three DOFs and manual/automatic control mode is proposed aiming to overcome the aforementioned limitations. The robot reaches the target nodules via the natural orifice and achieves biopsy sampling through the end-mounted surgical tools to elevate the diagnostic rate while improving safety during the operation. It is of significant significance in the face of the urgent demand for clinical minimally invasive surgery. The main contributions of this paper include the following:

- A flexible surgical robot for transbronchial biopsy is proposed. The robot has minimized size and supports both manual and automatic control modes. It also reserves the channel for surgical tools and endoscope, while maintaining adjustable stiffness of the end effector.
- The composition of the robotic system is introduced in detail. The kinematic model of the robot is deduced. Further, the robot prototype is fabricated, and the main motion performance and practical feasibility are verified by experiments.

The remainder of this paper is organized as follows. Section 2 presents the descriptions of the robotic system, including the overview of the system, the flexible mechanism, the actuation unit and operation procedures. Section 3 presents the kinematic analysis of the steerable snake-bone end effector. In Section 4, experimental evaluations are carried out, including the performance test and the test on the bronchial model. Section 5 is the discussion, and Section 6 is the conclusion of this work.

2. System descriptions

2.1. System overview

The robotic system consists of a slave-side manipulator, a mechanical arm, a master-side embedded box PC as the monitor and controller and a reserved channel placed in the slave-side manipulator (Fig. 1) for the insertion of surgical tools and the endoscope. Real-time image can be obtained through the endoscope installed in the reserved channel and displayed on the master-side PC for visual guidance and navigation. After reaching the target position, the endoscope can be extracted and replaced with surgical tools such as biopsy forceps, biopsy needle, cytologic brush, etc. The surgeons can control the slave-side manipulator via the master-side controller to perform the biopsy operation.

The complexity of the bronchial structure places more demands on the robot design. Hence, our proposed robotic system is devised to meet the following requirements and the main parameters of design requirements are listed in Table I:

- Minimized size. Network of bronchi is branching and decreasing continuously in size from the trachea to the alveoli. By the fifth generation, its diameter is only 3.5 mm [28]. To ensure that the robot can reach most expected positions, minimized size of the end effector and the flexible catheter are needed. In addition, enough space should also be reserved for the installation of the transmission system and vision units. Therefore, the size should be confined in a reasonable range.
- Sufficient flexibility and operability. The complex distribution network of bronchi requires sufficient flexibility and operability of the robot to execute accurate steering, forward and backward movements at the specified position.

Table I. Main parameters of design requirements.

Parameters	Value	Units
DOF	3	-
Required Channel	For surgical tools and for endoscope	-
Way to Enter Human Body	Transnasal/Transoral	-
Physical Property	Flexibility	-
Operating Mode	Automatically/Manually	-

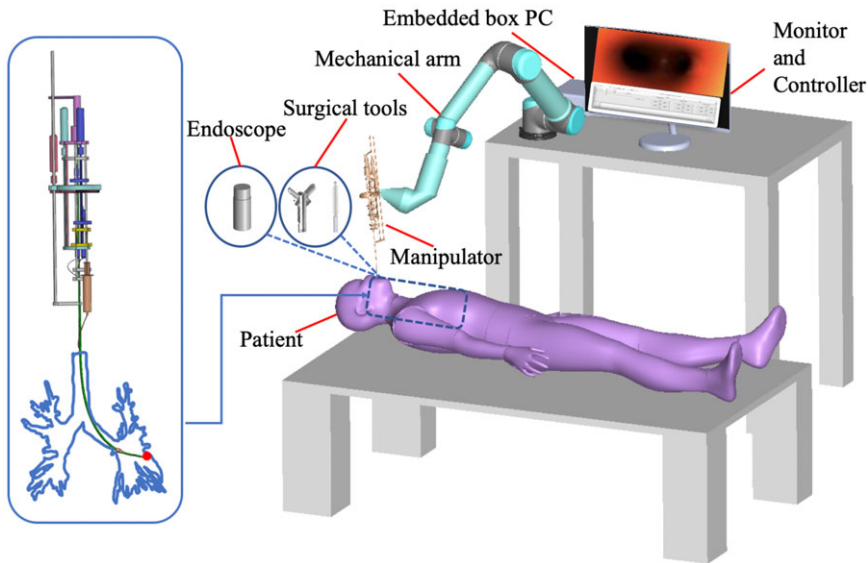


Figure 1. Overview of the flexible robotic system.

- Adaptability and stability. Since most scenes of the robot’s movement in the bronchus are constrained by bronchus walls [29], the end effector should get access and adjust stiffness to adapt to the different situations of the bronchus in smooth motion without causing trauma. Therefore, the catheter should be fixed at a specific position to make it stiffer while reducing jitter during the surgical operation.

2.2. Flexible mechanism

The flexible mechanism includes a steerable end effector and flexible catheters which is with compact structure, high space utilization and function realization.

According to the aforementioned design requirements, the steerable end effector adopts the structure of snake bone (diameter: 2.8 mm, length: 23.9 mm) which is composed of a base unit, ten snake-bone units and an end unit (Fig. 2(a)). The bending of the end effector can be achieved by the accumulation of small bending angles of each unit. Articulated joints can be regarded as sliding curved joints, which possess excellent performance in preventing transverse split, transverse slip, torsional stiffness, space efficiency [30, 31]. A channel (diameter: 1.4 mm) is reserved for the insertion of the endoscope or surgical tools. These two narrow channels are sandwiched between the internal catheter and the central channel while symmetrically distributing about the axis of the central channel. One end of the nickel-titanium (Ni-Ti) wire is fixed at the end unit of the end effector, with the other end passing through the narrow channel. Therefore, the curvature of the steerable effector can be controlled by altering the lengths of these two Ni-Ti wires.

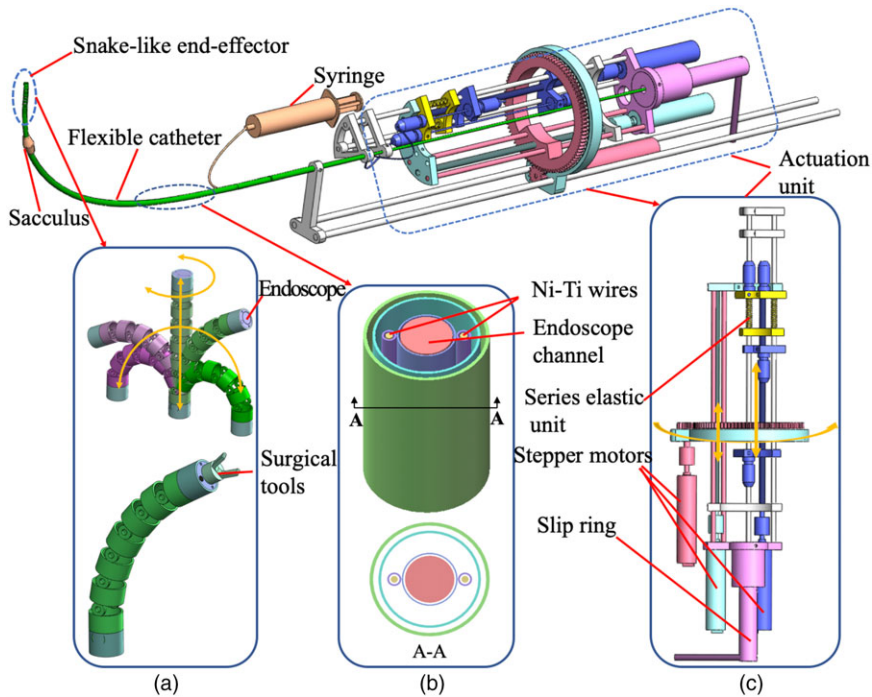


Figure 2. Composition of the robotic system. (a) The snake-bone end effector. (b) The flexible catheters. (c) The actuation unit.

The head-end of the flexible catheter, which is connected with the base unit of the steerable end effector, is with a stepped shaft to release the internal space to the greatest extent (Fig. 2(b)). The flexible catheter consists of an additional catheter (diameter: 3.4 mm), a main catheter (diameter: 2.7 mm), two Ni-Ti wires (diameter: 0.24 mm) as described, two catheters for Ni-Ti wires and the reserved channel. The length of the additional catheter is around 700 mm. One end of the additional catheter is fixed on the support. When it gets into bronchus together with the main catheter nested in it, the relatively large stiffness makes the additional catheter take the function of transmitting. Furthermore, the translation and rotation of the end effector are achieved via the relative movement of the additional catheter and the main catheter. A sacculus is attached to the outside of the additional catheter which expands under the pressure provided by a syringe, so that the catheter can be fixed at a specific position in the bronchus. The head-end of the syringe is connected with another similar sacculus forming a communicator for intraoperative observation.

2.3. Actuation unit

The actuation unit is used to execute bending, the translating and the rotating of the robot by varying the relative position of Ni-Ti wires and catheters (Fig. 2(c)). Two motors (RE13, Maxon motor, Inc.) are respectively connected with screws through the coupling. To achieve the bending and the translating motion, moving blocks with threaded hole are placed on the screw simultaneously, thus turning the rotational motion of the motor into translational motion. Another motor is connected with the gear to achieve the rotation. A series elastic unit is set on the front end, which changes the stiffness of the end effector by adjusting the stiffness coefficient of the spring. A conductive slip ring is set on the back end, from which the conductors and the reserved channel are led out to realize the static of the conductors during rotation. During the operation, the motion path of the bronchoscope robot can be planned in advance and entered into controller in combination with the preoperative image judgment

Table II. Notation used in this paper.

Name	Description
n	Index of the snake-bone units. $n = b$ at the base unit and $n = e$ at the end unit.
δ_i	Rotation angle of the Ni-Ti rope.
S	Arc-length parameter of the hypothetical primary backbone.
S_i	Arc-length parameter of the snake-bone unit.
$\rho(s)$	Radius of curvature of the hypothetical primary backbone.
$\rho_i(s)$	Radius of curvature of the snake-bone unit.
r	Radius of the snake-bone unit.
R	Radius of the hypothetical circle.
O_i	Center of the hypothetical circle.
θ_n	Rotation angle of upper plain of each snake-bone unit.
θ'_n	Hypothetical central angle.
ΔL	Elongation of Ni-Ti rope.
P_e	Coordinate of the end snake-bone unit.
\dot{x}	Time derivative of variable x .
J	Jacobian matrix.

and pathological analysis. The surgeon can switch to manual mode according to the actual circumstance in case potential medical accident happens.

2.4. Operation procedures

In the operation, the patient needs to adjust to the appropriate posture. After the confirmation, the series elastic unit is adjusted to the position with the minimal stiffness of the end effector. To begin with, the surgeon manually places the end effector close to the target. Meanwhile, the flexible mechanism is fixed on the robotic arm. Combined with preoperative medical image diagnosis and intraoperative real-time information, the doctor can control the end effector of the flexible robot to reach the targeting nodule automatically or manually. The sacculle will inflate when applying pressure to the syringe. After that, the flexible catheter is fixed and the series elastic unit is adjusted to the position with the maximal stiffness coefficient. At this time, surgeons can replace the endoscope with micro biopsy sampling tools via the reserved channel according to actual situation. Ultimately, to remove the surgical robot after sampling, the needed actions are contracting the sacculle by reducing the pressure of the one-way valve and adjusting the series elastic unit to the position with minimal stiffness coefficient.

3. Kinematic analysis

This section presents the kinematic analysis of the steerable snake-bone end effector. By controlling the relative length of two Ni-Ti wires, the end effector bends in the plane of Ni-Ti wires. The shape of the end effector is given by shape functions that is a solution of a system of nonlinear partial differential equations [32]. The analysis of kinematics refers to [33, 34]. Since each snake-bone unit is riveted to its neighbor, the length of the riveted section can be assumed to remain unchanged during movement. Then, the length of the central Ni-Ti wire is supposed to remain unchanged. Further assumptions are made to make the end effector model as simple as possible: (1) The gravity and friction of each unit at the end of snake bone are ignored. (2) Constraints by the bronchi that exist in reality are not considered here. (3) The mathematical description of the deformation between units is assumed to be countless continuous smooth functions.

Table II summarizes the notation used in this paper. Figure 3 shows the simplified analytical schematic diagram. The position and orientation of the end snake-bone unit relative to the base snake-bone unit

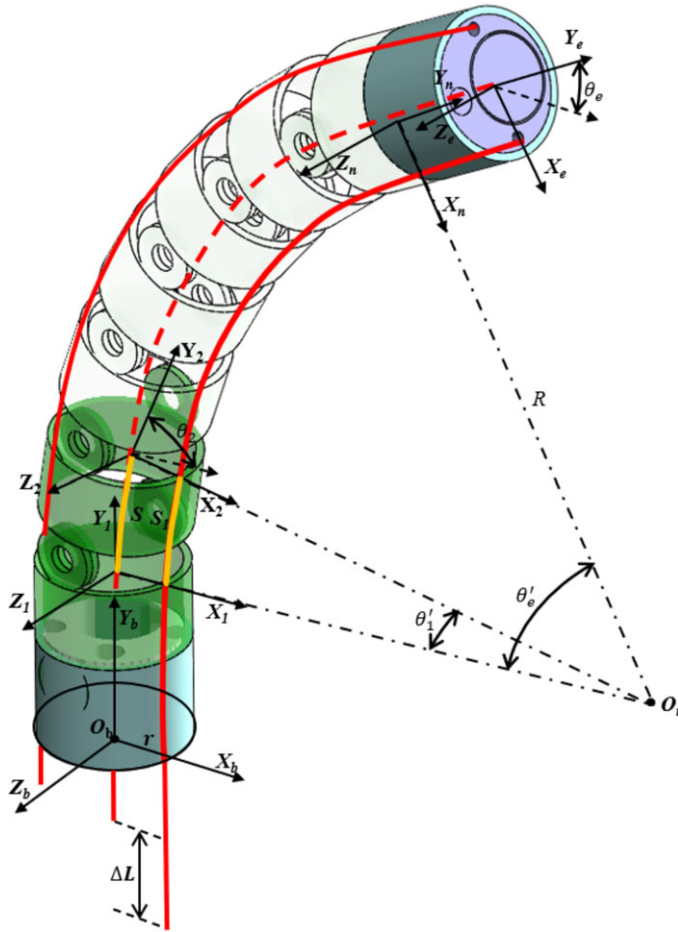


Figure 3. Schematic diagram of the end effector.

are expressed by two angles: δ and θ , where δ is the rotation angle relative to the line plane and θ is the rotation angle relative to the horizontal plane. According to the above assumptions, the arc-length of each continuous and smooth bending arc is given by

$$\rho(c) = \rho_i(c) + \Delta_i \tag{1}$$

where $\Delta_i = r \cos(\delta_i)$. Since there are only two Ni-Ti causing the bend, so $\delta_i = 0$.

Then, the arc-length between two adjacent snake-bone unit can be expressed as the integral of countless continuous smooth arcs:

$$S_i = \int ds_i = \int ds + \int ds_i - ds = S + \int (\rho_i(s) - \rho(s)) d\theta \tag{2}$$

$$S_i = S - \Delta_i \theta'_{i-1} = S - r \left(\frac{\Pi}{2} - (\theta_i - \theta_{i-1}) \right) \tag{3}$$

The rotating angles of all adjacent snake-bone elements are accumulated and derived as

$$\Delta L = \sum_{i=0}^n \left(r \left(\frac{\Pi}{2} - (\theta_i - \theta_{i-1}) \right) \right) = r \left(\frac{\Pi}{2} - (\theta_n - \theta_0) \right) \tag{4}$$

So the relationship between the length variation of Ni-Ti wire and the rotating angle of the end snake-bone unit can be derived, and the end effector can be bent to a configuration as follows:

$$\theta'_e = \frac{\Delta L}{r} \tag{5}$$

The hypothetical central angle is used to replace the above angle by

$$\theta'_{i-1} = \frac{\Pi}{2} - (\theta_i - \theta_{i-1}) \tag{6}$$

And the coordinate of the end snake-bone unit is given by

$$P_e \left(\frac{L_0}{\theta'_e} (1 - \cos \theta'_e), \frac{L_0}{\theta'_e} \sin \theta'_e, 0 \right) \tag{7}$$

The position and orientation of the end snake-bone unit can be presented by

$$\mathbf{u}_i = \left[\frac{L_0}{\theta'_e} (1 - \cos \theta'_e) \quad \frac{L_0}{\theta'_e} \sin \theta'_e \quad 0 \quad \phi_x \quad \phi_y \quad \phi_z \right]^T \tag{8}$$

$$\dot{\mathbf{u}}_i = \begin{bmatrix} \mathbf{J}_{ps} \\ \mathbf{J}_{\omega s} \end{bmatrix} \Delta L = \mathbf{J} \dot{\Delta L} \tag{9}$$

The Jacobian matrix can be obtained by taking the derivation of (8) to time and can be written by

$$\mathbf{J} = \begin{bmatrix} \frac{S_0}{\Delta L^2} \left(r \cos \frac{\Delta L}{r} + \Delta L \sin \frac{\Delta L}{r} - r \right) \\ \frac{S_0}{\Delta L^2} \left(\Delta L \cos \frac{\Delta L}{r} - r \sin \frac{\Delta L}{r} \right) \\ 0 \\ 0 \\ 0 \\ -\frac{1}{r} \end{bmatrix} \tag{10}$$

The results of the above kinematic analysis are used for reference of sensor-guided master-slave control which determines the position and posture of the end effector.

4. Experimental evaluation

4.1. Performance test

This test is set to evaluate the kinematical performance of the robotic system. Prototype of the robot is shown in Fig. 4. The flexible catheters of the prototype are composed of nested spring tubes with different wire diameters, and the actuation unit is mainly made of aluminum alloy. The end effector is placed on the standard coordinate scale plate so that the movement of the end effector can be observed more intuitively. The catheter is set up vertically and fixed on the 3D printed block, with the end effector extending by some length. The control program runs on the embedded box PC and communicates with the motor driver through the CAN bus. This test is to verify operating range of the robot under the master-slave control. According to the experimental results (Fig. 4(b)-(e)), the maximal bending angle is 180°, the longitudinal travel distance can reach 150 mm, and the robot can rotate up to 360°. In addition, as demonstrated in Fig. 4(c), the diameter of the sacculus will exceed 10 mm when it inflates under pressure so that it will stuck in the bronchus; thus, the use of sacculus can satisfy the need of fixing the catheter [28]. Main parameters of the proposed robot are listed in Table III.

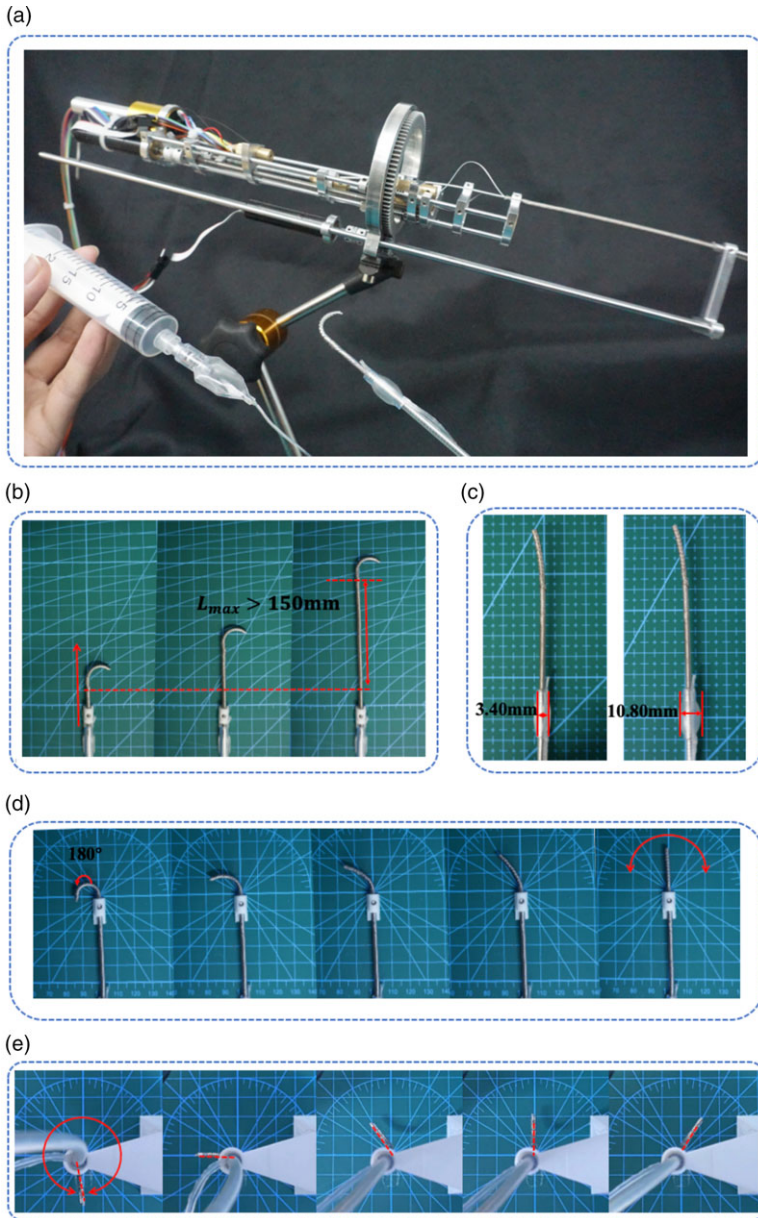


Figure 4. Prototype of the robotic system and results of the primitive experiment. (a) Prototype of the robotic system. (b) Translation maximum of the forward distance is longer than 150 mm. (c) Comparison: Sacculus with increasing pressure. (d) The steerable tip bends to 180° in two directions. (e) The steerable tip angles and rotates through 360°.

4.2. Test on the bronchial model

This test is to verify the practical feasibility of the robotic system by simulating the sampling operation of lung nodule biopsy in a bronchial model. Two target nodule locations were simulated in the bronchial model. The continuous movement of the robot is controlled by the manipulator. The process is observed including entering the bronchus, reaching the target nodule and retreating from the bronchus. Key frame images of the end effector movement process through the motion of advancing, rotating and bending

Table III. Main parameters of the proposed robot.

Parameters	Value	Units
DOF	3	-
Diameter of the End effector	2.8	mm
Diameter of the Surgical Tool Channel	1.4	mm
Length of the Insertion Part	700	mm
Maximal Travel Distance	150	mm
Maximal Bending Angle	180	deg
Maximal Rotational Angle	360	deg
Operating Mode	Automatically/Manually	-

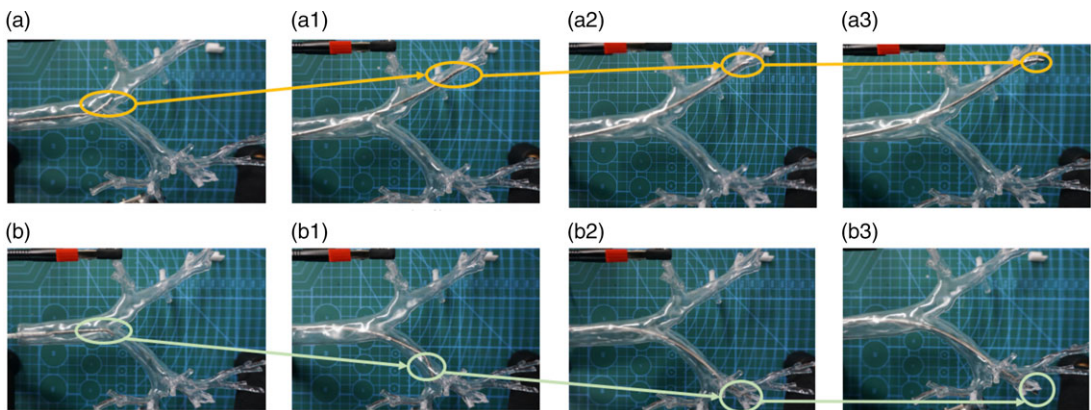


Figure 5. Process of test on the bronchial model. (a) and (b): The end effector is at the end of the trachea and ready to move forward inside the right/left main bronchi. (a1) and (b1) The end effector is at the end of the inferior lobar bronchus. (a2) and (b2): The end effector is at B^{10} (posterior basal bronchus). (a3) and (b3): The end effector reaches the B^{10c} bronchus.

of two representative routes are shown in Fig. 5(a)-(a3) and Fig. 5(b)-(b3). Figures in the first and third columns show the bending motion of the end effector. Figures in the second column show the translational motion of the end effector. Figures in the fourth column show both bending and rotating. The results show that the end effector and catheter of the robot can reach the target nodule through the narrow and complex bronchial tree, thus proving the feasibility of the robotic system.

5. Discussion

Based on the prototype of the robot platform, performance test and model-based test are carried out to demonstrate the features of the robot. As revealed in the experimental result, the end effector can reach a maximal bending angle of 180° and a maximal rotational angle of 360° . The insertion length of 700 mm and travel distance of 150 mm in the longitudinal direction can also be obtained. Hence, the final effects are generally satisfactory. Furthermore, the simulation of transbronchial lung biopsy is conducted on a model to verify the feasibility and effectiveness of the operation and the result indicates that the robotic system has met the clinical needs.

6. Conclusion

In this paper, a flexible surgical robotic system is proposed to meet the clinical requirements of transbronchial lung biopsy. Operation in narrow bronchus is completed by the designed steerable end effector

and flexible catheter which has high space utilization. To achieve the flexible operation of the end effector, the controller is carefully designed so that the transmission system can be actuated both manually and automatically. A mathematical model is established to analyze the kinematics of the steerable snake-bone end effector. The reserved channel can be used to install endoscope and different surgical tools. To ensure operation safety and maximize motion quality, a series elastic element is used in the system to adjust the stiffness and adaptability of the end effector in real time. A sacculus is integrated at certain position outside the catheter which can expand in bronchus when pressure is given, thus eliminating the jitter brought by operation. The operation procedures mentioned are described in detail.

Although the proposed robotic system has aforementioned advantages, several improvements ought to be made in the future. First, higher level of integration of the control system will be our focus in the next stage. For instance, fiber Bragg grating sensor and electromagnetic navigation system will be integrated into the robot system for more precise intraoperative feedback. Moreover, animal experiments and cadaveric experiments will be carried out in the future to evaluate the performance of the robotic system.

Supplementary materials. To view supplementary material for this article, please visit <https://doi.org/10.1017/S0263574722001345>.

Acknowledgement. We would like to thank Xiaotian Li and Jiali Sun for their enthusiastic help.

Authors' contributions. Changsheng Li and Xingguang Duan supervised the project; Changsheng li and Runtian Zhang designed the framework of the article; Runtian Zhang and Dongsheng Xie wrote the manuscript; Chao Qian revised the manuscript.

Financial support. This work is supported by the National Natural Science Foundation of China (No.62003045), the Beijing Municipal Natural Science Foundation-Haidian Primitive Innovation Joint Fund Project (No.L202021) and the Beijing Institute of Technology Research Fund Program for Young Scholars.

Conflicts of interest. There are no conflicts of interest, financial or other, for this manuscript.

Ethical considerations. There are no ethical considerations regarding this work.

References

- [1] A. Setio, F. Ciompi, G. Litjens, P. Gerke, C. Jacobs, S. Riel, M. Wille, M. Naqibullah, C. Sánchez and B. V. Ginneken, "Pulmonary nodule detection in ct images: False positive reduction using multi-view convolutional networks," *IEEE Trans. Med. Imaging* **35**(5), 1160–1169 (2016).
- [2] P. M. Ellis and R. Vandermeer, "Delays in the diagnosis of lung cancer," *J. Thorac. Dis.* **3**(3), 183–188 (2011).
- [3] D. F. Yankelevitz, A. P. Reeves, W. J. Kostis, B. Zhao and Henschke C. I., "Small pulmonary nodules: Volumetrically determined growth rates based on CT evaluation," *Radiology* **217**, 251–256 (2000).
- [4] C. I. Henschke, D. I. McCauley, D. F. Yankelevitz, D. P. Naidich, G. McGuinness, O. S. Miettinen, D. M. Libby, M. W. Pasmantier, J. Koizumi, N. K. Altorki and J. P. Smith, "Early lung cancer action project: Overall design and findings from baseline screening," *Lancet* **354**(9173), 99–105 (1999).
- [5] W. Mousa and M. Khan, "Lung Nodule Classification Utilizing Support Vector Machines," **In: Proceedings of the 2002 International Conference on Image Processing** (2002).
- [6] W. S. Krinsky, M. A. Pritchett and K. K. W. Lau, "Towards an optimization of bronchoscopic approaches to the diagnosis and treatment of the pulmonary nodules: A review," *J. Thorac. Dis.* **10**(S14), S1637 (2018).
- [7] S. P. Singh, D. S. Gierada, P. Pinsky, C. Sanders, N. Fineberg, Y. Sun, D. Lynch and H. Nath, "Reader variability in identifying pulmonary nodules on chest radiographs from the national lung screening trial," *J. Thorac. Imaging* **27**(4), 249–254 (2012).
- [8] S. Basu, L. O. Hall, D. B. Goldgof, Y. Gu, V. Kumar, J. Choi, R. J. Gillies and R. A. Gatenby, "Developing A Classifier Model for Lung Tumors in CT-Scan Images," **In: 2011 IEEE International Conference on Systems, Man, and Cybernetics** (2011) pp. 1306–1312.
- [9] Q. Dou, H. Chen, L. Yu, J. Qin and P.-A. Heng, "Multilevel contextual 3-D CNNs for false positive reduction in pulmonary nodule detection," *IEEE Trans. Biomed. Eng.* **64**(7), 1558–1567 (2017).
- [10] Y. Xie, Y. Xia, J. Zhang, Y. Song, D. Feng, M. Fulham and W. Cai, "Knowledge-based collaborative deep learning for benign-malignant lung nodule classification on chest ct," *IEEE Trans. Med. Imaging* **38**(4), 991–1004 (2019).

- [11] A. Tartar, A. Akan and N. Kilic, “A Novel Approach to Malignant-Benign Classification of Pulmonary Nodules By Using Ensemble Learning Classifiers,” *In: 2014 36th Annual International Conference of the IEEE Engineering in Medicine and Biology Society* (2014) pp. 4651–4654.
- [12] P. J. Swaney, A. W. Mahoney, A. A. Ramirez, E. Lamers, B. I. Hartley, R. H. Feins, R. Alterovitz and R. J. Webster, “Tendons, Concentric Tubes, and A Bevel Tip: Three Steerable Robots in One Transoral Lung Access System,” *In: 2015 IEEE International Conference on Robotics and Automation (ICRA)* (2015) pp. 5378–5383.
- [13] J. Memoli, P. J. Nietert and G. A. Silvestri, “Meta-analysis of guided bronchoscopy for the evaluation of the pulmonary nodule,” *Chest* **142**(2), 385–393 (2012).
- [14] F. Masaki, F. King, T. Kato, H. Tsukada, Y. Colson and N. Hata, “Technical validation of multi-section robotic bronchoscope with first person view control for transbronchial biopsies of peripheral lung,” *IEEE Trans. Biomed. Eng.* **68**(12), 3534–3542 (2021).
- [15] C. Li, X. Gu, X. Xiao, C. M. Lim and H. Ren, “Flexible robot with variable stiffness in transoral surgery,” *In: IEEE/ASME Trans. Mechatron.*, **25**(1), 1–10 (2020). doi: [10.1109/TMECH.2019.2945525](https://doi.org/10.1109/TMECH.2019.2945525).
- [16] F. J. Herth, M. Mayer, J. Thiboutot, C. M. Kapp and L. Yarmus, “Safety and performance of transbronchial cryobiopsy for parenchymal lung lesions,” *Chest* **160**(4), 1512–1519 (2021).
- [17] A. Heya, T. Kamegawa, T. Matsuno, T. Hiraki and A. Gofuku, “Development of Instantaneously Puncture System for Ct Fluoroscopy-Guided Interventional Radiology,” *In: 2016 IEEE/RSJ International Conference on Intelligent Robots and Systems (IROS)* (2016) pp. 2369–2374.
- [18] R. Nakadate, T. Iwasa, S. Onogi, J. Arata, S. Oguri, Y. Okamoto, T. Akahoshi, M. Eto and M. Hashizume, “Surgical robot for intraluminal access: An *ex vivo* feasibility study,” *Cyborg Bionic Syst.* **2020**, 1–9 (2020). doi: [10.34133/2020/8378025](https://doi.org/10.34133/2020/8378025).
- [19] P. E. Dupont, B. J. Nelson, M. Goldfarb, B. Hannaford, A. Mencias, M. K. O’Malley, N. Simaan, P. Valdastris and G.-Z. Yang, “A decade retrospective of medical robotics research from 2010 to 2020,” *Sci. Robot.* **6**(60), eabi8017 (2021).
- [20] C. Li, X. Gu, X. Xiao, C. M. Lim, X. Duan and H. Ren, “A flexible transoral robot towards covid-19 swab sampling,” *Front. Robot. AI* **8**, 51 (2021).
- [21] C. Li, Y. Yan, X. Xiao, X. Gu, H. Gao, X. Duan, X. Zuo, Y. Li and H. Ren, “A miniature manipulator with variable stiffness towards minimally invasive transluminal endoscopic surgery,” *IEEE Robot. Autom. Lett.* **6**(3), 5541–5548 (2021).
- [22] C. Li, X. Gu, X. Xiao, C. M. Lim and H. Ren, “A robotic system with multichannel flexible parallel manipulators for single port access surgery,” *IEEE Trans. Ind. Inform.* **15**(3), 1678–1687 (2019).
- [23] O. M. Omisore, S. Han, J. Xiong, H. Li, Z. Li and L. Wang, “A review on flexible robotic systems for minimally invasive surgery,” *IEEE Trans. Syst. Man Cybern. Syst.* **52**(1), 631–644 (2022).
- [24] K. Ohuchida, “Robotic surgery in gastrointestinal surgery,” *Cyborg Bionic Syst.* **2020**(1), 1–7 (2020). doi: [10.34133/2020/9724807](https://doi.org/10.34133/2020/9724807).
- [25] I. F. Zidane, Y. Khattab, S. Rezeki and M. El-Habrouk, “Robotics in laparoscopic surgery - A review,” *Robotica* **21**, 1–48 (2022).
- [26] S. Amack, M. F. Rox, J. Mitchell, T. E. Ertop and R. J. Webster, “Design and Control of A Compact Modular Robot for Transbronchial Lung Biopsy,” *In: Image-Guided Procedures, Robotic Interventions, and Modeling* (2019).
- [27] L. Dupourqué, F. Masaki, Y. L. Colson, T. Kato and N. Hata, “Transbronchial biopsy catheter enhanced by a multisection continuum robot with follow-the-leader motion,” *Int. J. Comput. Assist. Radiol. Surg.* **14**(5), 2021–2029 (2019).
- [28] T. J. Pedley, R. C. Schroter and M. F. Sudlow, “The prediction of pressure drop and variation of resistance within the human bronchial airways,” *Respir. Physiol.* **9**(3), 387–405 (1970).
- [29] S. D. Murgu, “Robotic assisted-bronchoscopy: Technical tips and lessons learned from the initial experience with sampling peripheral lung lesions,” *BMC Pulm. Med.* **19**(1), 395 (2019).
- [30] F. Jelínek, E. A. Arkenbout, P. Henselmans, R. Pessers and P. Breedveld, “Classification of joints used in steerable instruments for minimally invasive surgery—A review of the state of the art,” *J. Med. Devices* **8**(1), 030914 (2015).
- [31] J. Zhang, Q. Fang, P. Xiang, D. Sun, Y. Xue, R. Jin, K. Qiu, R. Xiong, Y. Wang, H. Lu, “A survey on design, actuation, modeling, and control of continuum robot,” *Cyborg Bionic Syst.* **2022**(4), 1–13 (2022). doi: [10.34133/2022/9754697](https://doi.org/10.34133/2022/9754697).
- [32] C. Li and C. D. Rahn, “Design of continuous backbone, cable-driven robots,” *J. Mech. Des.* **124**(2), 265–271 (2002).
- [33] N. Simaan, R. Taylor and P. Flint, “A Dexterous System for Laryngeal Surgery,” *In: IEEE International Conference on Robotics and Automation, Proceedings. ICRA '04*, vol. **1**, (2004) pp. 351–357.
- [34] C. Yang, H. Xu, X. Li and F. Yu, “Kinematic modeling and solution of rigid-flexible and variable-diameter underwater continuous manipulator with load,” *Robotica* **40**(4), 1020–1035 (2022).